Superconducting fluctuations and the Nernst effect: A diagrammatic approach

Iddo Ussishkin
Department of Physics, Princeton University, Princeton, New Jersey 08544, USA
(Received 18 November 2002; revised manuscript received 28 February 2003; published 30 July 2003)

We calculate the contribution of superconducting fluctuations above the critical temperature T_c to the transverse thermoelectric response α_{xy}, the quantity central to the analysis of the Nernst effect. The calculation is carried out within the microscopic picture of BCS, and to linear order in magnetic field. We find that as $T \to T_c$, the dominant contribution to α_{xy} arises from the Aslamazov-Larkin diagrams, and is equal to the result previously obtained from a stochastic time-dependent Ginzburg-Landau equation [I. Ussishkin, S. L. Sondhi, and D. A. Huse, Phys. Rev. Lett. **89**, 287001 (2002)]. We present an argument which establishes this correspondence for the heat current. Other microscopic contributions, which generalize the Maki-Thompson and density of states terms for the conductivity, are less divergent as $T \to T_c$.

DOI: 10.1103/PhysRevB.68.024517 PACS number(s): 74.40.+k, 74.25.Fy, 72.15.Jf

I. INTRODUCTION AND DISCUSSION OF RESULTS

In a superconductor, fluctuations of the superconducting order parameter above the transition temperature T_c affect various properties such as the magnetic susceptibility and transport coefficients. The study of superconducting fluctuations has a long history (for reviews, see, e.g., Refs. 1,2). More recently, interest in fluctuation phenomena was renewed with the discovery of high-temperature superconductors, where their short coherence lengths, high critical temperatures, and layered structures imply a large regime for the observation of fluctuations.[3]

One experiment that has aroused particular interest recently is that of the Nernst effect. In this experiment, a temperature gradient $(-\nabla T)\|\hat{\mathbf{x}}$ is applied in the presence of a magnetic field $\mathbf{B}\|\hat{\mathbf{z}}$, and the electric field response (in the absence of transport electric current) is measured in the $\hat{\mathbf{y}}$ direction. Below T_c in the vortex state the Nernst effect is large due to vortex motion, while in the normal state it is typically very small. In experiments in low-temperature superconductors, no sign of superconducting fluctuations was reported as the temperature was raised above T_c.[4] In contrast, several different experiments did observe the appearance of a fluctuation tail above the critical temperature in the Nernst signal of the high-temperature superconductors[5–8] (and also in the related Ettinghausen effect[9]). More recently, the Nernst effect above T_c has attracted considerable attention with measurements showing a sizeable Nernst signal well above T_c, in particular in the underdoped regime.[10,11]

While a Nernst experiment is carried out under open circuit conditions, the transport coefficients, which arise naturally in a theoretical description, are those which relate the transport electric and heat currents to the electric field and temperature gradient,

$$\begin{pmatrix} \mathbf{j}_{\mathrm{tr}}^{e} \\ \mathbf{j}_{\mathrm{tr}}^{Q} \end{pmatrix} = \begin{pmatrix} \sigma & \alpha \\ \tilde{\alpha} & \kappa \end{pmatrix} \begin{pmatrix} \mathbf{E} \\ -\nabla T \end{pmatrix}. \tag{1}$$

Here, σ is the conductivity tensor, κ is a tensor of thermal conductivity, and α, $\tilde{\alpha}$ are the thermoelectric tensors (which obey the Onsager relations $\tilde{\alpha} = T\alpha$). Applying the open circuit condition to Eq. (1), the Nernst coefficient is expressed in terms of the conductivity and thermoelectric tensors,

$$\nu_N = \frac{E_y}{(-\nabla T)_x B} = \frac{1}{B} \frac{\alpha_{xy}\sigma_{xx} - \alpha_{xx}\sigma_{xy}}{\sigma_{xx}^2 + \sigma_{xy}^2}. \tag{2}$$

The transverse thermoelectric response α_{xy}, the quantity on which this paper is focused, is of primary interest for understanding the effect of superconducting fluctuations on the Nernst signal (as discussed below).

In a recent paper, Sondhi, Huse, and the present author discussed the contribution of superconducting fluctuations to the thermoelectric and thermal conductivity tensors using a stochastic time-dependent Ginzburg-Landau equation (TDGL) in the limit of Gaussian fluctuations.[12] In this paper, we revisit the calculation of the transverse thermoelectric response α_{xy} using a diagrammatic calculation within the BCS theory. The details of this calculation are presented in subsequent sections. In the remainder of this section, we present and discuss the results of this paper.

We calculate α_{xy} above the critical temperature T_c, to linear order in the magnetic field $\mathbf{B}\|\hat{\mathbf{z}}$, and to leading order in $T - T_c$. We find that, in two and three dimensions (2D and 3D), the contribution of superconducting fluctuations to the transverse thermoelectric response is

$$\alpha_{xy}^{\mathrm{AL}} = \begin{cases} \dfrac{1}{6\pi} \dfrac{e}{\hbar} \dfrac{\xi(T)^2}{\ell_B^2} \propto \dfrac{1}{T - T_c} & \text{for 2D,} \\ \dfrac{1}{12\pi} \dfrac{e}{\hbar} \dfrac{\xi(T)}{\ell_B^2} \propto \dfrac{1}{\sqrt{T - T_c}} & \text{for 3D.} \end{cases} \tag{3}$$

Here, $\ell_B = (\hbar c/eB)^{1/2}$ is the magnetic length and $\xi(T) \propto (T - T_c)^{-1/2}$ is the coherence length of the superconducting order parameter.

It is well known (see, e.g., Refs. 1,2) that superconducting fluctuations enhance the conductivity above T_c due to both the Aslamazov-Larkin[13] and the Maki-Thompson[14,15] contributions (there are also density of states terms, which are less important for the conductivity). A similar identification of the microscopic contributions applies to other transport coefficients. In the case of the transverse thermoelectric response, as the superscript in Eq. (3) suggests, we find that the leading order contribution to α_{xy} is due to the Aslamazov-Larkin diagrams alone. The contribution of the Maki-Thompson and density of states diagrams is less divergent as $T \to T_c$.

Physically, the Aslamazov-Larkin diagrams correspond to the contribution of thermal fluctuations of the order parameter. Their contribution to α_{xy} may be viewed either as the transport heat current carried by such fluctuations when they respond to an electric field, or as the transport electric current carried by the fluctuations as they respond to a temperature gradient (all in the presence of the magnetic field). The same physics is identically described by the Gaussian approximation to a stochastic TDGL. (We will have more to remark on the correspondence between the two approaches in subsequent sections.) Indeed, the result obtained in this paper, Eq. (3), is identical to the result obtained in the Gaussian approximation to the stochastic TDGL in Ref. 12.[16]

The calculations in this paper are carried out assuming particle-hole symmetry, i.e., neglecting any contributions which arise due to asymmetry around the Fermi surface in properties such as the density of states. Particle-hole symmetry implies that $\sigma_{xy}=\alpha_{xx}=\kappa_{xy}=0$ (and therefore in the calculation of these transport coefficients, it is necessary to break particle-hole symmetry). The conventional result for α_{xy} in the normal metallic state also vanishes in this limit. However, it is important to note that this result is not required by symmetry, and will not necessarily hold when additional processes are taken into account (without breaking the particle-hole symmetry). Indeed, as we find in this paper, and as is evident in calculations using a stochastic TDGL,[12,17] the contribution of superconducting fluctuations to α_{xy} does not vanish in the particle-hole symmetric limit. As the assumption of particle-hole symmetry is a very good approximation for a BCS superconductor, it is therefore well justified in the present case.

A second assumption made in this paper is that the order parameter has *s*-wave symmetry. In the context of the high-temperature superconductors, it is of interest to consider also the case of *d*-wave symmetry in this approach. We note here that this will not affect the conclusions of this paper. The results of the stochastic TDGL would still correspond to the Aslamazov-Larkin contribution; and the arguments showing that the Maki-Thompson and density of states terms are less divergent remain valid in this case as well.[18] (We do not consider here the related issue of whether nodal quasiparticles, which appear when the temperature is lowered and the condensate is formed, contribute to α_{xy}.)

We now return to the discussion of the Nernst coefficient ν_N. As noted in Eq. (2), ν_N is related to both the conductivity and the thermoelectric tensors. However, the main effect of superconducting fluctuations on the Nernst signal above T_c is due to α_{xy}. Indeed, the contribution of fluctuations to the second term in the numerator of Eq. (2) is small due to considerations of particle-hole symmetry. Moreover, not too close to T_c, the conductivity is dominated by the normal-state contribution. It follows that the main contribution of superconducting fluctuations to the Nernst signal (to linear order in B) is $\alpha_{xy}^{\mathrm{AL}}/\sigma_{xx}$, with σ_{xx} being the normal-state contribution.

Since the result for $\alpha_{xy}^{\mathrm{AL}}$, Eq. (3), depends only on the coherence length $\xi(T)$, and in a simple manner, a comparison with experiment should apparently be straightforward. In Ref. 12, such a comparison for a high-temperature superconductor was presented. On the other hand, in low-temperature superconductors, for which the BCS theory is certainly applicable, the appearance of the fluctuation tail in the Nernst signal was not previously reported to the best of our knowledge.[4] The reason for this is that low-temperature superconductors are typically also good conductors in the normal state. Consequently, $\alpha_{xy}^{\mathrm{AL}}/\sigma_{xx}$, the contribution of superconducting fluctuations to the Nernst signal, is strongly suppressed in bulk low-temperature superconductors.

The situation can be improved considerably by looking at a thin film, which is effectively a two-dimensional superconductor if the coherence length is larger than the film thickness. First, the fluctuation tail of α_{xy} is enhanced by going to lower dimensionality, as is evident in Eq. (3). [The result for two dimensions in Eq. (3) is to be divided by the film thickness to obtain the result for a thin film.] Second, such films may have a significantly lower normal state conductivity. Taken together, these effects may considerably enhance the contribution of fluctuations to the Nernst signal. A similar situation may occur in a layered structure with weak coupling between the layers and with a low normal-state conductivity, as is the case for the high-temperature superconductors.[12]

In closing this section, we note that a diagrammatic calculation of α_{xy} was previously attempted by Varlamov and Livanov,[19] but was unfortunately marred by an incorrect treatment of the heat current vertex. We also note an important aspect of the calculation of α_{xy}, namely, the role of *bulk magnetization currents*, and the need to subtract their contribution[20] (discussed in the present context in Sec. II A). As discussed in Ref. 12, this issue was largely overlooked in the literature.

In the remainder of this paper, we present the details of our calculation. In Sec. II, we present the Kubo formula for α_{xy}, and discuss the contribution of bulk magnetization currents. For completeness, we also present known results for the propagator of superconducting fluctuations. The diagrams that appear in the calculation of α_{xy}, and the physics they describe, are discussed in Sec. III. In Sec. IV, we discuss the calculation of the heat current vertex. A general argument regarding its calculation is given, establishing the correspondence to the heat current in the TDGL. In Sec. V, we calculate the Aslamazov-Larkin diagrams, and obtain Eq. (3). The Maki-Thompson and density of states diagrams are considered in Sec. VI. Finally, we summarize our discussion in Sec. VII.

II. FORMALISM

A. Kubo formula for α_{xy}

In this section, we discuss the linear-response theory for the transverse thermoelectric response. We present the Kubo formula for α_{xy}, and discuss the role of bulk magnetization currents and the subtraction of their contribution.

The thermoelectric tensor is considered in this paper by calculating the heat current response to an electric field. Alternatively, one could consider within the linear response theory the electric current response to Luttinger's ''gravitational field.''[21] The result for α_{xy} is, of course, independent of which formulation is used, and results are presented in terms of one of them only for convenience.

The heat current response to an electric field is related to the heat current-electric current correlator by using the standard Kubo formula. Here, we are interested in the calculation of this response to linear order in the magnetic field. This amounts to introducing an additional current vertex coupled to the magnetic field.[22] Here, we present this result as the Kubo formula for the linear response to both an electric and a magnetic field. The electric field $\mathbf{E}\|\hat{\mathbf{x}}$ and the magnetic field $\mathbf{B}\|\hat{\mathbf{z}}$ are introduced at finite frequency and wavevector, respectively, using the vector potential

$$\mathbf{A}=\frac{c\mathbf{E}}{i\Omega}e^{-i\Omega t}+\frac{B\hat{\mathbf{y}}}{iQ}e^{iQ\hat{\mathbf{x}}\cdot\mathbf{r}}. \tag{4}$$

The heat current in the $\hat{\mathbf{y}}$ direction, in response to the electric and magnetic fields (in the dc limit), is given by

$$\frac{j_y^Q}{EB}=-\lim_{\Omega,Q\to 0}\frac{1}{\Omega Qc}\mathrm{Re}[\Lambda(Q,\Omega_m)]\big|_{i\Omega_m\to\Omega+i0}. \tag{5}$$

Here, the three current correlator Λ is defined by

$$\Lambda(Q,\Omega_m)=\int_0^\beta d\tau d\tau' e^{i\Omega_m\tau}\int d\mathbf{r}d\mathbf{r}' e^{iQ\hat{\mathbf{x}}\cdot(\mathbf{r}'-\mathbf{r})} \times\langle T_\tau j_y^Q(\mathbf{r},\tau)j_y^e(\mathbf{r}',\tau')j_x^e(0)\rangle, \tag{6}$$

where $\Omega_m=2\pi mT$ is a bosonic Matsubara frequency (with units in which $\hbar=k_B=1$), and the upper limit of integration over imaginary times τ and τ' is the inverse temperature $\beta=1/T$. In Eq. (5), an analytic continuation of Ω_m to real frequencies is performed before the zero-frequency limit is taken.

An important aspect of the calculation of the transverse thermoelectric response, discussed in detail by Cooper, Halperin, and Ruzin,[20] is the need to account for *bulk magnetization currents*. This issue arises because the microscopic electric and heat currents, as calculated by the Kubo formula, are composed of transport and magnetization currents,

$$\mathbf{j}^e=\mathbf{j}^e_{\mathrm{tr}}+\mathbf{j}^e_{\mathrm{mag}},\quad \mathbf{j}^Q=\mathbf{j}^Q_{\mathrm{tr}}+\mathbf{j}^Q_{\mathrm{mag}}. \tag{7}$$

The magnetization currents are currents that circulate in the sample and do not contribute to the net currents which are measured in a transport experiment. On the other hand, they do contribute to the total microscopic currents, and it is thus necessary to subtract them from the total currents to obtain the transport current response. In the presence of an applied electric field, it was shown in Ref. 20 that the magnetization current is given by

$$\mathbf{j}^Q_{\mathrm{mag}}=c\mathbf{M}\times\mathbf{E}, \tag{8}$$

where $\mathbf{M}$ is the equilibrium magnetization (in the absence of the electric field). It then follows that the transverse thermoelectric response is given by

$$\tilde{\alpha}_{yx}=-\tilde{\alpha}_{xy}=\frac{j_y^Q}{E}-cM_z, \tag{9}$$

where j_y^Q/E is found using the Kubo formula, Eqs. (5) and (6). Using the Onsager relations $\alpha_{xy}=\tilde{\alpha}_{xy}/T$.

It is evident from Eq. (9) that α_{xy} is obtained by subtracting the result of two independent calculations: the response of the total current to the applied electric and magnetic fields, and the magnetization currents as derived from the equilibrium magnetization. We note that these terms cannot be combined (to the best of our knowledge) into a single Kubo formula, since one cannot write a local operator for the magnetization or transport currents separately, only for the total currents.

Therefore, we need the equilibrium magnetization $\mathbf{M}$ for the calculation of α_{xy}. Diagrammatically, it may be calculated to linear order in B by considering the current response to a magnetic field at a finite wavevector,

$$\mathbf{M}=-\hat{\mathbf{z}}\lim_{Q\to 0}\frac{B}{Q^2c^2}\mathrm{Re}[\Pi(Q)], \tag{10}$$

where

$$\Pi(Q)=\int_0^\beta d\tau\int d\mathbf{r}e^{-iQ\hat{\mathbf{x}}\cdot\mathbf{r}}\langle T_\tau j_y^e(\mathbf{r},\tau)j_y^e(0)\rangle. \tag{11}$$

The contribution of superconducting fluctuations to the magnetization is well known.[1,2,23] In this paper, we will thus use the known results for the magnetization, and concentrate on the calculation of Eqs. (5) and (6) for the total current response.

As mentioned above, the calculation of α_{xy} may proceed via the alternative route of calculating the electric current response to a ''gravitational field'' ψ. In this case, a similar situation arises, where in order to obtain the transport current the electric magnetization current has to be subtracted. The latter is given in this case by[20]

$$\mathbf{j}^e_{\mathrm{mag}}=-c\mathbf{M}\times\boldsymbol{\nabla}\psi. \tag{12}$$

In Ref. 12, the total heat current response to an electric field and the total current response to a temperature gradient were calculated using the stochastic TDGL. The apparent discrepancy between the results for the total currents and the Onsager relations was invoked to demonstrate the need of subtracting out the magnetization currents. In contrast, in the linear-response formalism the calculation for the electric current yields its response to a gravitational field gradient, and this apparent discrepancy does not arise. The magnetization

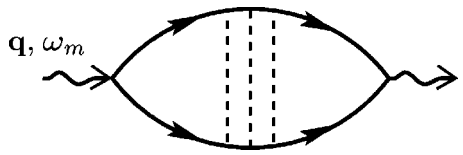

FIG. 1. Diagram for the noninteracting two-particle propagator $\Pi(\mathbf{q},\omega_m)$. Lines with arrows are electronic Green functions, and disorder is shown in the ladder approximation by dashed lines.

currents (and the total currents) trivially obey the same Onsager relations obeyed by the transport currents. Nevertheless, the magnetization currents must be subtracted to obtain the correct result for the transport coefficients.

B. Fluctuation propagator

The contribution of superconducting fluctuations to the current correlator in Eq. (6) is calculated in this paper for a BCS superconductor (with *s*-wave symmetry), with Hamiltonian

$$\mathcal{H}=\sum_{\mathbf{k},\sigma}\epsilon_{\mathbf{k}}c^{\dagger}_{\mathbf{k},\sigma}c_{\mathbf{k},\sigma}+\sum_{\mathbf{k},\mathbf{q},\sigma}U_{\mathbf{q}}c^{\dagger}_{\mathbf{k}+\mathbf{q},\sigma}c_{\mathbf{k},\sigma}+\lambda\sum_{\mathbf{k},\mathbf{k}',\mathbf{q}}c^{\dagger}_{\mathbf{k}',\uparrow}c^{\dagger}_{-\mathbf{k}'+\mathbf{q},\downarrow}c_{-\mathbf{k}+\mathbf{q},\downarrow}c_{\mathbf{k},\uparrow}. \tag{13}$$

Here, $\epsilon_{\mathbf{k}}=k^2/2m$ is the kinetic energy of the electrons, $\sigma=\uparrow,\downarrow$ is their spin, $U_{\mathbf{q}}$ is the disorder potential (with the usual Gaussian distribution), and $\lambda<0$ is the attractive BCS interaction (where only states with energy differing from the Fermi energy by at most ω_D participate in the interaction term). The relevant diagrams for superconducting fluctuations are calculated using the finite-temperature diagrammatic technique. This approach is analogous to the one used in the case of the conductivity, leading to the Aslamazov-Larkin[13] and Maki-Thompson[14,15] contributions. (For a detailed account of the diagrammatic calculation of the conductivity, see, e.g., Ref. 2.) A basic ingredient of the diagrammatic calculation is the propagator of superconducting fluctuations L. For the sake of completeness, we present here the known results for L.

Accounting for the electron-electron interaction in the ladder approximation, the fluctuation propagator L is related to the noninteracting two-particle propagator Π through

$$L(\mathbf{q},\omega_m)=[\lambda^{-1}-\Pi(\mathbf{q},\omega_m)]^{-1} \tag{14}$$

(see Fig. 1 for the diagram of Π). To obtain the retarded fluctuation propagator, the Matsubara frequency is analytically continued to the real axis ($i\omega_m\to\omega+i0$) and Π is calculated to leading order in $\mathbf{q}$ and ω. Assuming particle-hole symmetry, the retarded fluctuation propagator is then

$$L^R(\mathbf{q},\omega)=-\frac{1}{\nu}\frac{1}{\epsilon+\eta q^2-i\omega\tau_{\rm BCS}} \tag{15}$$

(and the advanced fluctuation propagator is $L^A(\mathbf{q},\omega)=[L^R(\mathbf{q},\omega)]^*$). In Eq. (15), ν is the density of states per spin, $\epsilon=\ln(T/T_c)\approx(T-T_c)/T_c$ is the reduced temperature, $\tau_{\rm BCS}=\pi/8T_c$, and

$$\eta=-D\tau_{\rm el}\left[\psi\left(\frac{1}{2}+\frac{1}{4\pi T_c\tau_{\rm el}}\right)-\psi\left(\frac{1}{2}\right)-\frac{1}{4\pi T_c\tau_{\rm el}}\psi'\left(\frac{1}{2}\right)\right]. \tag{16}$$

Here, $\tau_{\rm el}$ is the elastic scattering time, $D=v_F^2\tau_{\rm el}/d$ is the diffusion constant (for d dimensions), and $\psi(x)$ is the digamma function. The parameters in Eq. (15) are directly related to the coefficients appearing in a TDGL for the order parameter. In particular, $\xi(T)=\sqrt{\eta/\epsilon}$ is the superconducting coherence length and $\tau_{\rm BCS}$ is the relaxation time for the order parameter fluctuations.

III. DIAGRAMS AND INTERPRETATION

In this section, we present the diagrams which appear in the calculation of the correlator (6), and discuss the physical processes which they represent. For this purpose, the microscopic picture is perhaps best recast in terms of a quantum functional integral approach.[25,24] We begin this section by briefly discussing this approach.

The expectation value of a current operator $\mathbf{j}$ (which can be either the electric current or the heat current) in response to a driving field ϕ may be expressed in terms of an imaginary time functional integral

$$\langle\mathbf{j}\rangle=\frac{\int D\psi D\bar{\psi}\mathbf{j}e^{-S[\psi,\bar{\psi},\phi]}}{\int D\psi D\bar{\psi}e^{-S[\psi,\bar{\psi},\phi]}}. \tag{17}$$

Here, ψ and $\bar{\psi}$ are the fermion fields, and the action S is given by

$$S=\int_0^{\beta}d\tau\int d\mathbf{x}\left[\sum_{\sigma}\bar{\psi}_{\sigma}(x)\partial_{\tau}\psi_{\sigma}(x)+\mathcal{H}(x)\right], \tag{18}$$

where β is the inverse temperature, $x=(\mathbf{x},\tau)$, and $\mathcal{H}$ is the Hamiltonian density. Introducing a pairing field Δ via the usual Hubbard-Stratonovich transformation, the expectation value of the current may be rewritten as

$$\langle\mathbf{j}\rangle=\frac{\int D\Delta D\bar{\Delta}\langle\mathbf{j}\rangle_{\Delta\bar{\Delta}\phi}e^{-S_{\rm eff}[\Delta,\bar{\Delta},\phi]}}{\int D\Delta D\bar{\Delta}e^{-S_{\rm eff}[\Delta,\bar{\Delta},\phi]}}. \tag{19}$$

Here, $S_{\rm eff}$ is the effective action for the pairing field which is obtained by integrating out the fields ψ (Ref. 26) and

$$\langle\mathbf{j}\rangle_{\Delta\bar{\Delta}\phi}=\frac{\int D\psi D\bar{\psi}\mathbf{j}e^{-S_0[\psi,\bar{\psi},\phi]+\int d\tau d\mathbf{x}(\Delta\bar{\psi}_{\uparrow}\bar{\psi}_{\downarrow}+\bar{\Delta}\psi_{\downarrow}\psi_{\uparrow})}}{\int D\psi D\bar{\psi}e^{-S_0[\psi,\bar{\psi},\phi]+\int d\tau d\mathbf{x}(\Delta\bar{\psi}_{\uparrow}\bar{\psi}_{\downarrow}+\bar{\Delta}\psi_{\downarrow}\psi_{\uparrow})}}, \tag{20}$$

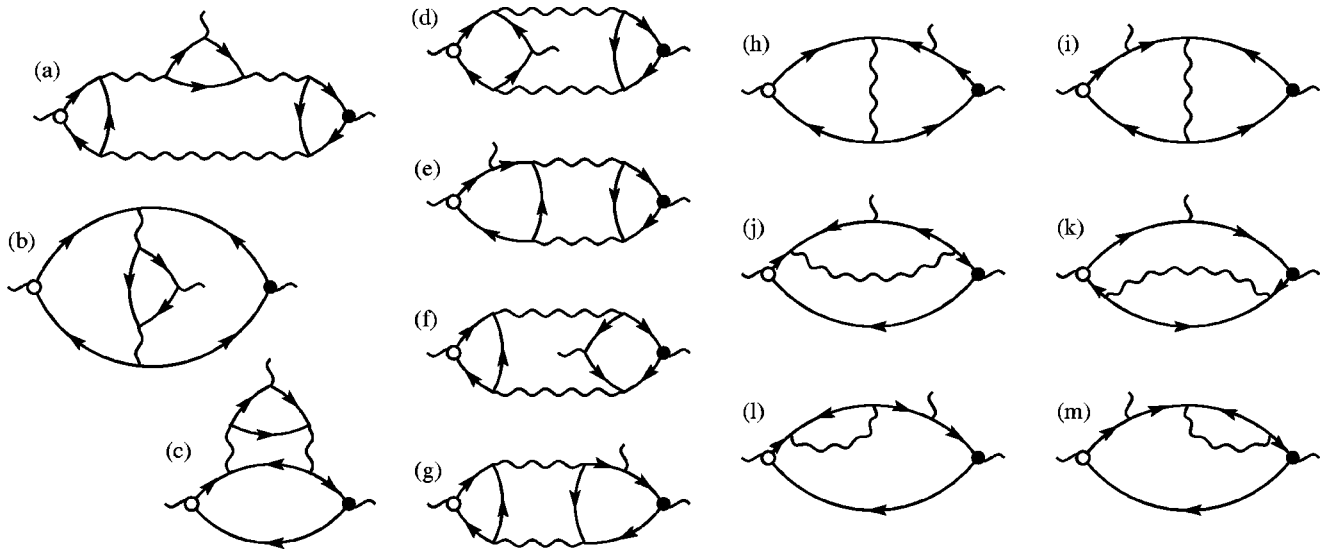

FIG. 2. Diagrams arising in the calculation of the transverse thermoelectric response [see Eqs. (5)–(6)]. A wavy line represents the fluctuation propagator, and the lines with arrows are the electronic Green functions. The vertices are the heat current vertex j_y^Q (open circle), the electric current vertex coupled to the electric field j_x^e (full circle), and the electric current vertex coupled to the magnetic field j_y^e (no circle). ''Mirror image'' diagrams, which may be obtained by reversing the arrow direction on each of the electronic Green functions in the diagrams above [except diagrams (b), (d), and (f), for which the mirror image is not a new diagram], are not presented [See Fig. 4 below for the mirror image of diagram (a)]. Also not presented are the different possibilities of adding disorder to each of these diagrams.

where S_0 is the part of the action S which is quadratic in ψ. The calculation of the contribution of superconducting fluctuations to the current proceeds by applying a Gaussian approximation to Eq. (19). More specifically, this involves expanding both $S_{\rm eff}[\Delta,\bar{\Delta},\phi]$ and $\langle \mathbf{j}\rangle_{\Delta\bar{\Delta}\phi}$ to second order in Δ and $\bar{\Delta}$.

Consider first the calculation of the conductivity, in which case ϕ is the electric field. In Eq. (19), the field appears in two places, namely, in $\langle \mathbf{j}\rangle_{\Delta\bar{\Delta}\phi}$ and in the effective action $S_{\rm eff}[\Delta,\bar{\Delta},\phi]$. The Aslamazov-Larkin approximation involves keeping the field dependence in the effective action only. The resulting expression is equivalent to a calculation using a stochastic TDGL also done at Gaussian order. The quantity $\langle \mathbf{j}\rangle_{\Delta\bar{\Delta}}$ is the current associated with the order parameter configuration. The response of the order parameter to the field is described by the effective action, which is identical to the TDGL description. In particular, note that, in the TDGL, the electric field is coupled to linear order to the current associated with the order parameter, as is described by the Aslamazov-Larkin diagram. Not included in the Aslamazov-Larkin approximation are the terms obtained by keeping the field in $\langle \mathbf{j}\rangle_{\Delta\bar{\Delta}\phi}$. These describe corrections to the normal-state response modified by the presence of the order parameter, and are the Maki-Thompson and density of states corrections.

The situation for the transverse thermal response is somewhat different than it is for the conductivity as we are considering the linear response to two fields (since we are considering the heat current response to both electric and magnetic fields). The resulting diagrams are presented in Fig. 2 (in most cases, the diagrams have ''mirror images'' which are not presented in the figure, but are, of course, also taken into account). Before proceeding a word on nomenclature, while the situation here is a bit different than in the case of the conductivity, we will refer to the diagrams corresponding to the TDGL contribution as the Aslamazov-Larkin diagrams; all other diagrams will be collectively referred to as Maki-Thompson and density of states diagrams, although they do not correspond to corrections to the normal-state transverse thermoelectric response only, as discussed below.

The diagram in Fig. 2(a) and its ''mirror image'' are the Aslamazov-Larkin diagrams, which correspond to the contribution of the stochastic TDGL. To obtain these diagrams, the electric and magnetic fields are retained in the effective action in Eq. (19) only, and the average over the current operator (which in this case, is the average over the heat current operator, $\langle \mathbf{j}^Q\rangle_{\Delta\bar{\Delta}}$) gives the heat current associated with the order parameter configuration. Moreover, the motion of the order parameter described by these diagrams is that of the TDGL, with the electric and magnetic fields coupled to linear order to the electric currents associated with the order parameter configuration. This correspondence will be revisited below. In Sec. IV, we discuss the heat current associated with the motion of the order parameter $\langle \mathbf{j}^Q\rangle_{\Delta\bar{\Delta}}$ and its connection to the heat current in the TDGL. In Sec. V, we calculate the Aslamazov-Larkin diagrams for α_{xy} and find that they give the same contribution as that found using a stochastic TDGL in Ref. 12.

The rest of the diagrams describe a variety of processes which involve corrections to normal-state properties, and may be understood along similar lines. Diagrams (b) and (c) of Fig. 2 describe a correction to the normal-state thermoelectric response due to the order parameter fluctuations, with Maki-Thompson [diagram (b)] and density of state [dia-

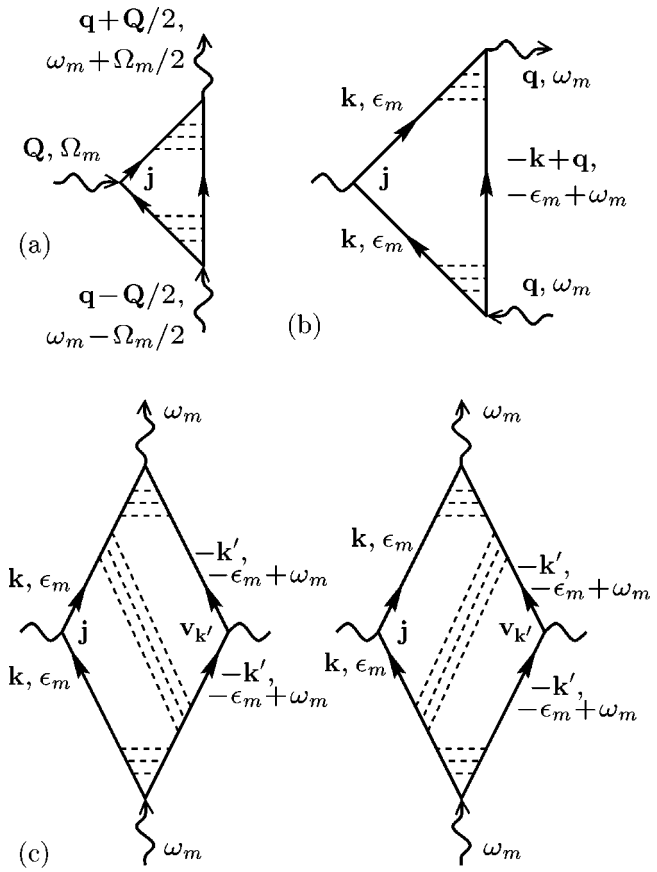

FIG. 3. Diagrams used in the text for evaluation of the current vertices $\mathbf{J}^e$ and $\mathbf{J}^Q$ appearing in the Aslamazov-Larkin diagrams. Lines with arrows are electronic Green functions, and dashed lines denote disorder, shown here in the ladder approximation. The microscopic current vertex $\mathbf{j}$ represents either the electric current vertex $\mathbf{j}^e=-e\mathbf{v}_\mathbf{k}$ or the heat current vertex $\mathbf{j}^Q=i\epsilon_m\mathbf{v}_\mathbf{k}$.

gram (c)] contributions, but with the order parameter responding to linear order to the magnetic field. Likewise, diagrams (d) and (e) describe the normal-state response to a magnetic field in the presence of superconducting fluctuations affected by the electric field. Diagrams (f) and (g) describe the heat current associated with an order parameter configuration (as in the Aslamazov-Larkin diagrams), but with the dynamics of the order parameter modified by a term not captured by the TDGL. (It is interesting to note that in the microscopic picture, there are corrections to the TDGL in the order parameter motion in this case.) Finally, diagrams (h)–(m) describe corrections to the normal-state transverse thermoelectric response α_{xy}.

IV. RELATION BETWEEN CURRENT VERTICES

In this section, we consider the calculation of the triangular block appearing in the Aslamazov-Larkin diagram [see Fig. 3(a)]. In this diagram, the microscopic current vertex $\mathbf{j}$ can be either an electric current vertex $\mathbf{j}^e$ or a heat current vertex $\mathbf{j}^Q$. This diagram corresponds to the current in the presence of an order parameter configuration, and is thus directly related to the current which appears in the TDGL. Accordingly, while the microscopic current vertex is denoted with $\mathbf{j}$, we denote the current vertex presented by the diagram in Fig. 3(a) with $\mathbf{J}$.

The result for the electric current vertex $\mathbf{J}^e$ is well known (and is needed, e.g., for the conductivity[13]). Our main concern here is with the heat current vertex $\mathbf{J}^Q$, for which we establish the following result: At $Q=\Omega_m=0$ [for conventions regarding incoming and outgoing energies and momenta, see Fig. 3(a)], the electric and heat current vertices are related by

$$\mathbf{J}^Q=-\frac{i\omega_m}{2e}\mathbf{J}^e. \tag{21}$$

Heuristically, this form is expected for a preformed pair of charge $-2e$; but this is the BCS limit, for which an explicit calculation is needed. Together with the known result for $\mathbf{J}^e$ [see Eq. (24) below], this allows the calculation of the Aslamazov-Larkin diagrams in Sec. V, as well as obtaining the expression for the heat current in the TDGL.[12]

For completeness, we consider first the calculation of the electric current vertex $\mathbf{J}^e$. The vertex $\mathbf{J}^e$ is needed in the calculation of the Aslamazov-Larkin diagram to leading order in external frequencies and momenta, and it is thus sufficient to set the external frequencies to zero, $\Omega_m=\omega_m=0$, and consider linear order in the wavevectors $\mathbf{q}$ and $\mathbf{Q}$. There is no linear term in $\mathbf{Q}$; indeed, it is straightforward to show that $\mathbf{J}^e(q=\Omega_m=\omega_m=0)$ is symmetric in $\mathbf{Q}$.[27] In the calculation of the electric current vertex, we thus set $Q=\Omega_m=\omega_m=0$, and calculate the vertex to linear order in $\mathbf{q}$, $\mathbf{J}^e(\mathbf{q})$.

Setting $Q=\Omega_m=\omega_m=0$ in $\mathbf{J}^e$, the diagram for the electric current vertex is as in Fig. 3(b), but with $\omega_m=0$ (and $\mathbf{j}=\mathbf{j}^e=-e\mathbf{v}_\mathbf{k}$, where $\mathbf{v}_\mathbf{k}=\mathbf{k}/m$). The same diagram may be obtained by inserting an electric current vertex in the diagram for $\Pi(\mathbf{q},\omega_m=0)$, given in Fig. 1 (and correctly accounting for the spin indices). Using the relation

$$\boldsymbol{\nabla}_\mathbf{k}G(\mathbf{k},\epsilon_m)=\mathbf{v}_\mathbf{k}G(\mathbf{k},\epsilon_m)^2, \tag{22}$$

where $G(\mathbf{k},\epsilon_m)$ is the electron Green function, the following result is obtained:

$$\mathbf{J}^e=-2e\boldsymbol{\nabla}_\mathbf{q}\Pi(\mathbf{q},\omega_m=0). \tag{23}$$

Note the appearance of the Cooper pair charge, $-2e$ (denoted below as e^*). The expansion of Eq. (23) to linear order in $\mathbf{q}$ gives the result for the electric current vertex,[13]

$$\mathbf{J}^e(\mathbf{q})=-4e\,\eta\nu\mathbf{q} \tag{24}$$

(η and ν were defined in Sec. II B). The familiar expression for the electric current in the TDGL (in the absence of fields) follows from this result. More precisely, Eq. (24) is the electric current associated with a pairing field configuration $\Delta=e^{i\mathbf{q}\cdot\mathbf{r}}$, using

$$\mathbf{J}^e=e^*\eta\nu[\Delta^*(-i\boldsymbol{\nabla}\Delta)+\text{c.c.}]. \tag{25}$$

[The conventional TDGL form, with $1/2m^*$ replacing $\eta\nu$ (as in, e.g., Ref. 1), is obtained after rescaling the pairing field.]

We now reconsider the calculation of the electric current vertex, this time with an arbitrary ω_m, as a first step towards establishing Eq. (21). Setting $Q=\Omega_m=0$, the electric current vertex $\mathbf{J}^e$ is presented in Fig. 3(b) (with $\mathbf{j}=\mathbf{j}^e=-e\mathbf{v_k}$). Using Eq. (22), the expansion of $\mathbf{J}^e$ to linear order in $\mathbf{q}$ is equivalent to introducing a second velocity vertex. The vertex $\mathbf{J}^e$ is then written as $\mathbf{q}$ times the contribution of square diagrams as in Fig. 3(c) (with $\mathbf{j}=\mathbf{j}^e$). The following observation follows from the structure of these diagrams: To linear order in $\mathbf{q}$, but at an arbitrary ω_m, the electric current vertex has the structure

$$\mathbf{J}^e=-e\mathbf{q}\sum_{\epsilon_m} f(\epsilon_m,-\epsilon_m+\omega_m), \tag{26}$$

where the function f results from integration over all internal momenta in the diagrams. The function f depends only on the energy variables appearing in the electronic Green functions, and running along the two sides of the diagrams (we use here the fact that disorder scattering is elastic). In addition, because of the symmetric structure of the diagrams in Fig. 3(c), we have

$$f(\epsilon_m,-\epsilon_m+\omega_m)=f(-\epsilon_m+\omega_m,\epsilon_m). \tag{27}$$

The structure of the result for $\mathbf{J}^e$ as presented in Eqs. (26) and (27) is sufficient for establishing Eq. (21) to linear order in $\mathbf{q}$; it is unnecessary to evaluate f explicitly.

As with the electric current vertex, for the calculation of the Aslamazov-Larkin diagram, we only need the heat current vertex $\mathbf{J}^Q$ to leading order in wavevectors and frequencies. As it turns out [cf. Eq. (21)], this is one order higher than the leading order in $\mathbf{J}^e$. By symmetry of the structure of the diagrams for the current vertices, they are invariant under $\mathbf{Q},\Omega_m\to-\mathbf{Q},-\Omega_m$. For the expansion of $\mathbf{J}^Q$, this shows that there is no term linear in $\mathbf{Q}$ or Ω_m alone, but does not exclude a term proportional to $\mathbf{Q}\Omega_m$. In the calculation below, we use the fact that in the Aslamazov-Larkin diagrams [Fig. 2(a) and its mirror image], we need the heat current vertex in the $\hat{\mathbf{y}}$ direction, perpendicular to $\mathbf{Q}\|\hat{\mathbf{x}}$, and thus do not consider such a term.

We thus proceed by setting $Q=\Omega_m=0$. The heat current vertex $\mathbf{J}^Q$ is then given in Fig. 3(b) (with $\mathbf{j}=\mathbf{j}^Q=i\epsilon_m\mathbf{v_k}$; see comments at the end of this section). As in the case of the electric current vertex $\mathbf{J}^e$, the expansion of $\mathbf{J}^Q$ to linear order in $\mathbf{q}$ amounts to the introduction of a second velocity vertex, resulting in square diagrams as in Fig. 3(c) (with $\mathbf{j}=\mathbf{j}^Q$). It follows from the structure of these diagrams that to linear order in $\mathbf{q}$ (and at an arbitrary ω_m), the heat current vertex has the structure

$$\mathbf{J}^Q=\mathbf{q}\sum_{\epsilon_m} i\epsilon_m f(\epsilon_m,-\epsilon_m+\omega_m), \tag{28}$$

where the function f results from integration over all internal momenta in the diagrams. The important point here is that the function f that appears in Eq. (26) is *identical* to the one that appears in Eq. (28). Equation (28) may be rewritten as

$$\mathbf{J}^Q=\mathbf{q}\sum_{\epsilon_m}\left(i\epsilon_m-\frac{i\omega_m}{2}\right)f(\epsilon_m,-\epsilon_m+\omega_m) + \mathbf{q}\sum_{\epsilon_m}\frac{i\omega_m}{2}f(\epsilon_m,-\epsilon_m+\omega_m). \tag{29}$$

Here, the first term on the right-hand side can be shown to vanish using Eq. (27). On comparing the second term with Eq. (26), we find the relation between the current vertices, Eq. (21).

We note that to this order of the calculation $\mathbf{J}^Q$ does not have a branch cut after an analytic continuation of $i\omega_m$ to the ω plane. After the analytic continuation, we thus have to linear order in $\mathbf{q}$ and ω

$$\mathbf{J}^Q(\mathbf{q},\omega)=-\frac{\omega}{2e}\mathbf{J}^e(\mathbf{q})=2\eta\nu\omega\mathbf{q}. \tag{30}$$

This result is used below in the calculation of the Aslamazov-Larkin diagrams, and may be used to obtain the heat current in the TDGL[12] (again, note the appearance of the Cooper pair charge $-2e$). To be precise, Eq. (30) is the heat current associated with a pairing field configuration $\Delta=e^{i\mathbf{q}\cdot\mathbf{r}-i\omega t}$, using [cf. Eq. (25)]

$$\mathbf{J}^Q=-\eta\nu\left[\frac{\partial\Delta^*}{\partial t}\boldsymbol{\nabla}\Delta+\text{c.c.}\right]. \tag{31}$$

Previously, the heat current vertex $\mathbf{J}^Q$ was considered by several authors, beginning with the work of Caroli and Maki.[28] However, Eqs. (21) and (30) do not appear to have been obtained previously (i.e., before Ref. 12) with the correct factor.[29] The same result may, of course, be obtained by an explicit (but more cumbersome) calculation of the heat current vertex $\mathbf{J}^Q$. However, in addition to their being more straightforward, the arguments presented in this section have the advantage of being very general, applicable to arbitrary disorder strength and range. [Note that the important ingredient used to obtain Eqs. (26)–(28) is just the absence of inelastic scattering.] Finally, we have shown here that Eq. (21) holds to linear order in $\mathbf{q}$; we note that the argument may be extended to higher orders in $\mathbf{q}$ as well.

In the remainder of this section, we comment briefly on the microscopic heat current vertex $\mathbf{j}^Q$ used in the calculation. The microscopic energy current operator, and therefore the microscopic heat current operator, has two different representations—see, e.g., Ref. 30. The first involves a time derivative,

$$\hat{\mathbf{j}}^Q=\frac{1}{2}\sum_{\mathbf{k},\sigma}[\mathbf{v}_\mathbf{k}c^\dagger_{\mathbf{k},\sigma}(i\partial_t-\mu)c_{\mathbf{k},\sigma}+\text{H.c.}], \tag{32}$$

leading to the microscopic heat current vertex (at zero wavevector and frequency) $\mathbf{j}^Q=i\epsilon_m\mathbf{v}_\mathbf{k}$ used above. The second representation uses the equation of motion for the electronic operators to replace the time derivative with the Hamiltonian (13), leading to the heat current operator[31]

$$\hat{\mathbf{j}}^Q=\sum_{\mathbf{k},\sigma}(\epsilon_\mathbf{k}-\mu)\mathbf{v}_\mathbf{k}c^\dagger_{\mathbf{k},\sigma}c_{\mathbf{k},\sigma}+\sum_{\mathbf{k},\mathbf{q},\sigma}U_\mathbf{q}\mathbf{v}_\mathbf{k}c^\dagger_{\mathbf{k}+\mathbf{q}/2,\sigma}c_{\mathbf{k}-\mathbf{q}/2,\sigma}$$
$$+\lambda\sum_{\mathbf{k},\mathbf{k}',\mathbf{q}}\frac{\mathbf{q}}{m}c^\dagger_{\mathbf{k}',\uparrow}c^\dagger_{-\mathbf{k}'+\mathbf{q},\downarrow}c_{-\mathbf{k}+\mathbf{q},\downarrow}c_{\mathbf{k},\uparrow}. \tag{33}$$

The three terms in Eq. (33) represent the contribution to the heat current of the kinetic energy, the disorder potential, and the interaction energy, respectively. Diagrammatically, the second (third) terms give rise to vertices where the disorder (interaction) lines connect with the fermion lines. If this representation is used for the microscopic heat current operator, one obtains several different diagrams contributing to $\mathbf{J}^Q$.[31] However, the result for $\mathbf{J}^Q$ is identical whether Eq. (32) or (33) is used for the microscopic heat current operator, as we have verified explicitly in both the clean and the disordered limits. In our discussion above, we have used Eq. (32) as it is of a much simpler form, and can be used to obtain Eq. (21) using the general arguments presented above.

V. CALCULATION OF THE ASLAMAZOV-LARKIN DIAGRAMS

In this section, we calculate the Aslamazov-Larkin contribution to α_{xy}. The starting point is the expression for the Aslamazov-Larkin diagrams depicted in Fig. 4. To leading order in momentum and energy, the current vertices depend only on momentum and energy flowing from one fluctuation propagator to the other, as in Eqs. (24) and (30). It follows that the Aslamazov-Larkin contribution to the current correlator Λ [see Eq. (6)] is given by

$$\Lambda^{\mathrm{AL}}(Q,i\Omega_m)=-\frac{1}{\beta}\sum_{\omega_m}\int\frac{d\mathbf{q}}{(2\pi)^d}\{J^e_x(q_x+Q)J^e_y(q_y)J^Q_y(q_y,i\omega_m+i\Omega_m/2)L(\mathbf{q},i\omega_m)L(\mathbf{q}+Q\hat{\mathbf{x}},i\omega_m)L(\mathbf{q}+Q\hat{\mathbf{x}},i\omega_m+i\Omega_m)$$
$$+J^e_x(q_x)J^e_y(q_y)J^Q_y(q_y,i\omega_m+i\Omega_m/2)L(\mathbf{q},i\omega_m)L(\mathbf{q},i\omega_m+i\Omega_m)L(\mathbf{q}+Q\hat{\mathbf{x}},i\omega_m+i\Omega_m)\}. \tag{34}$$

Following the standard procedure, the sum over Matsubara frequencies may be expressed as an integral over the contour presented in Fig. 5. The resulting expression, after the analytic continuation $i\Omega_m\to\Omega+i0$, is given by

$$\Lambda^{\mathrm{AL}}(Q,\Omega)=-\frac{1}{\pi}\int_{-\infty}^{\infty}d\omega n(\omega)\int\frac{d\mathbf{q}}{(2\pi)^d}(J^e_x(q_x+Q)J^e_y(q_y)\{J^Q_y(q_y,\omega+\Omega/2)L^R(\mathbf{q}+Q\hat{\mathbf{x}},\omega+\Omega)\mathrm{Im}[L^R(\mathbf{q},\omega)L^R(\mathbf{q}+Q\hat{\mathbf{x}},\omega)]$$
$$+J^Q_y(q_y,\omega-\Omega/2)L^A(\mathbf{q},\omega-\Omega)L^A(\mathbf{q}+Q\hat{\mathbf{x}},\omega-\Omega)\mathrm{Im}[L^R(\mathbf{q}+Q\hat{\mathbf{x}},\omega)]\}$$
$$+J^e_x(q_x)J^e_y(q_y)\{J^Q_y(q_y,\omega+\Omega/2)L^R(\mathbf{q},\omega+\Omega)L^R(\mathbf{q}+Q\hat{\mathbf{x}},\omega+\Omega)\mathrm{Im}[L^R(\mathbf{q},\omega)]$$
$$+J^Q_y(q_y,\omega-\Omega/2)L^A(\mathbf{q},\omega-\Omega)\mathrm{Im}[L^R(\mathbf{q},\omega)L^R(\mathbf{q}+Q\hat{\mathbf{x}},\omega)]\}). \tag{35}$$

Here, $n(\omega)=\frac{1}{2}\coth(\omega/2T)$, and $L^R(\mathbf{q},\omega)$ and $L^A(\mathbf{q},\omega)$ are the analytic continuation of $L(\mathbf{q},i\omega_m)$ on the two sides of the cut at $\mathrm{Im}\omega=0$. The main contribution to the integrals is from small wavevectors and frequencies; to leading order in $T-T_c$, $n(\omega)\approx T/\omega$, and the fluctuation propagator L and current vertices $\mathbf{J}^e$ and $\mathbf{J}^Q$ are given by Eqs. (15), (24), and (30), respectively. Next, the expression is expanded to linear order in Q and Ω, the integrals are calculated, and using Eq. (5), we obtain for two and three dimensions,

$$\frac{j^Q_y}{E}=\begin{cases}-\dfrac{e^2TB}{2\pi c}\dfrac{\eta}{\epsilon} & \text{for 2D,}\\ -\dfrac{e^2TB}{4\pi c}\sqrt{\dfrac{\eta}{\epsilon}} & \text{for 3D.}\end{cases} \tag{36}$$

With the identification of the superconducting coherence length $\xi(T)=\sqrt{\eta/\epsilon}$, this result is identical to the one obtained by considering the Gaussian fluctuations in a stochastic TDGL.[12,17]

As discussed in Sec. II A, it is necessary to subtract the magnetization current $\mathbf{j}^Q_{\mathrm{mag}}=c\mathbf{M}\times\mathbf{E}$ from this result to obtain the correct transport response. The corresponding contribution of superconducting fluctuations to the magnetization is given by[1,2]

$$\mathbf{M}=\begin{cases}-\dfrac{e^2TB}{3\pi c^2}\dfrac{\eta}{\epsilon} & \text{for 2D,}\\ -\dfrac{e^2TB}{6\pi c^2}\sqrt{\dfrac{\eta}{\epsilon}} & \text{for 3D.}\end{cases} \tag{37}$$

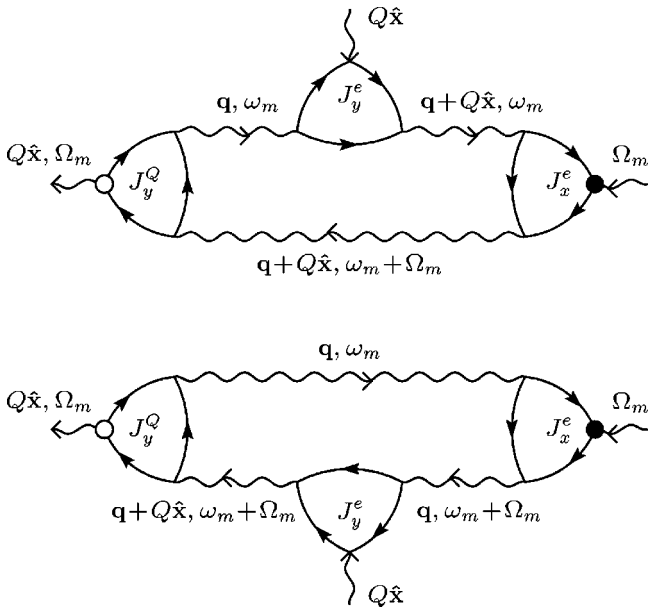

FIG. 4. Aslamazov-Larkin diagrams contributing to j_y^Q/EB [See Eqs. (5)–(6)]. The wavy lines correspond to the fluctuation propagator L; electric and heat current vertices are indicated in the figure.

We note that in the Aslamazov-Larkin calculation, the magnetization currents contribute two thirds of the total current in both two and three dimensions.

The final result for the Aslamazov-Larkin contribution to α_{xy} is obtained after the subtraction of the magnetization currents. The result is given in Eq. (3), where we introduce back $\hbar$, and present the result in terms of the coherence length $\xi(T)=\sqrt{\eta/\epsilon}$.

VI. MAKI-THOMPSON AND DENSITY OF STATES TERMS

In this section, we consider the Maki-Thompson and density of states diagrams [diagrams (b)–(m) in Fig. 2]. We show here that these terms are less divergent than the Aslamazov-Larkin diagrams as $T\rightarrow T_c$. In addition, a similar conclusion can be drawn for the magnetization. We thus find that in the microscopic calculation of α_{xy}, the Aslamazov-Larkin result, Eq. (3), is the most divergent contribution as $T\rightarrow T_c$.

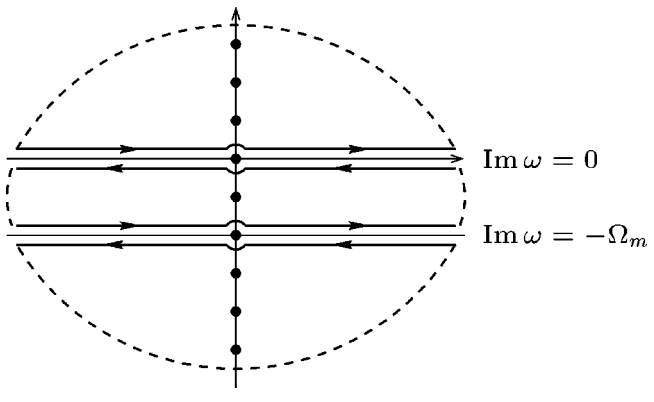

FIG. 5. Contour in the complex ω plane used for expressing the sum over Matsubara frequencies ω_m in Eq. (34) as an integral, leading to Eq. (35). The contour runs along the cuts of $L(\mathbf{q},\omega)$ and $L(\mathbf{q},\omega+i\Omega_m)$, and is closed at a distance from the origin which is taken to infinity. The dots are the poles of $n(\omega)$ at $i\omega_m$.

We note that a similar result may or may not hold for different transport coefficients, and each case must be examined separately. Indeed, in the case of the conductivity in three dimensions, the Maki-Thompson contribution has the same divergence as the Aslamazov-Larkin contribution.[14] In two dimensions the Maki-Thompson diagram diverges at any temperature in a naive calculation, a divergence which is regularized by introducing a pair breaking mechanism.[15,32,33] After this regularization, the Maki-Thompson contribution has a form which is somewhat different than the power law of the Aslamazov-Larkin term, and its ultimate divergence is only logarithmic. Nevertheless, this is an important microscopic contribution to the conductivity (except very close to T_c). In contrast, a different situation may hold for other transport properties. For example, it was recently argued that the Maki-Thompson and density of states terms for the thermal conductivity (first discussed in Ref. 34) lead to a nondiverging contribution.[35]

The method that we use here to obtain our result is that of power counting, applied to each of the diagrams independently. We thus avoid the explicit calculation of the diagrams, which would be needed if subleading terms are desired. In each of these diagrams, after each of the electronic blocks is calculated, the structure that remains is that of an integral over momentum and energy, with the integrand being composed of fluctuation propagators and electronic blocks. We apply power counting arguments to this integral to find the dependence of each diagram on the reduced temperature ϵ. (This procedure does not exclude the possibility that the coefficient of this power is actually zero and that the power of the diagram is therefore lower, nor does it exclude the possibility that the diagram is identically zero.)

For the purpose of clarification, we begin by considering the Aslamazov-Larkin diagram [Fig. 2(a)], which was calculated explicitly in Sec. V. The power counting is thus applied to Eq. (35); we now count powers of ϵ in the integral explicitly. In the integrand, there are three fluctuation propagators L (contributing a power ϵ^{-1} each), two electric current vertices $\mathbf{J}^e$ ($\epsilon^{1/2}$ each), and one heat current vertex $\mathbf{J}^Q$ ($\epsilon^{3/2}$). To obtain j_y^Q/EB [see Eq. (5)], the integral is expanded in external frequency Ω (ϵ^{-1}) and external wavevector Q ($\epsilon^{-1/2}$). The integration over momentum gives another $\epsilon^{d/2}$, while there is no contribution associated with the integration over energy [because of the $n(\omega)$ factor]. Accounting for all contributions, we obtain a divergence of $\epsilon^{d/2-2}$. Similar arguments give an identical result for the divergence of the magnetization, giving $\alpha_{xy}^{\mathrm{AL}}\propto\epsilon^{d/2-2}$, in agreement with our exact calculation, Eq. (3).

Next we consider diagrams (b)–(g) in Fig. 2. In these diagrams, the number of fluctuation propagators is one less than in the Aslamazov-Larkin diagram. If any of these diagrams is to be as divergent as the Aslamazov-Larkin diagram, then this loss of a power of ϵ^{-1} must be compensated

(as it is in the case of the Maki-Thompson diagram in the conductivity). A power of ϵ^{-1} is regained when considering the electronic block of the diagram which has two microscopic current vertices in it, provided they are in the same direction. Here, this will only occur for diagrams (d) and (e), in which the two vertices which are in the same block are j_y^e and j_y^Q. Indeed, in the Aslamazov-Larkin diagram, the vertices J_y^e and J_y^Q contribute ϵ^2. In diagrams (d) and (e), the block containing the vertices j_y^e and j_y^Q contributes only one power of ϵ.[36] Moreover, for these two diagrams to diverge as the Aslamazov-Larkin diagram, the expansion in external wavevector Q and external frequency Ω should give powers of $\epsilon^{-1/2}$ and ϵ^{-1}, respectively, as it does for the Aslamazov-Larkin diagram. The expansion in Ω indeed gives a power of ϵ^{-1}, since the external frequency appears explicitly in the fluctuation propagator (and also due to a diffusive pole as in the case of the Maki-Thompson conductivity diagram). However, the important point in this analysis is that in diagrams (d) and (e), the expansion in external momentum Q does not gain a power of $\epsilon^{-1/2}$, but instead accounts for $\epsilon^{1/2}$ in the power counting. The reason for this is that the external momentum, which flows from the j_y^e vertex to the j_y^Q vertex, does not flow through the fluctuation propagators of the diagram. The expansion in external momentum is thus limited to the electron block which includes these two vertices, where it is straightforward to check that expansion in the external momentum leads to a power of $\epsilon^{1/2}$. Finally, diagrams (h)–(m) involve only one fluctuation propagator and will clearly be less divergent than the Aslamazov-Larkin term.

We have demonstrated by power counting arguments that while the Aslamazov-Larkin diagram, Fig. 2(a), diverges as $\epsilon^{d/2-2}$, all other diagrams in Fig. 2 are less divergent as $T \to T_c$. Similar arguments hold for the fluctuation contribution to the magnetization, and hence for α_{xy}. In view of this conclusion, we do not calculate the Maki-Thompson and density of diagrams explicitly. [We note that diagrams (b)–(g) in Fig. 2, as well as the Maki-Thompson and density of states diagrams in the calculation of the magnetization, will have a logarithmic divergence in two dimensions as $T \to T_c$.]

VII. CONCLUSIONS

The main result of this paper is that the leading contribution in the microscopic calculation of α_{xy} arises from the Aslamazov-Larkin diagrams, which correspond to the contribution of Gaussian fluctuations in the stochastic TDGL. The Maki-Thompson and density of states terms are less divergent as $T \to T_c$. In concluding this paper, we comment on several aspects of this result.

It is well known that in calculating the contribution of superconducting fluctuations to the conductivity, the Aslamazov-Larkin diagrams correspond to the Gaussian approximation of a stochastic TDGL.[1,2] In establishing the correct form for the heat current vertex in Sec. IV, we verify this correspondence also for thermal transport.

There are two directions in which the calculation may be extended beyond this approximation: by considering the additional microscopic contributions (as we did in this paper), or by going beyond the Gaussian approximation in the stochastic TDGL (cf. Ref. 12). We would like to emphasize that these approaches are of a very different nature, and their regime of validity is also different.

The stochastic TDGL is traditionally understood as the model for the critical dynamics of a superconductor (model *A* in the classification of Hohenberg and Halperin[37]). As such, the TDGL should give the relevant contribution as the temperature approaches T_c in the critical regime (which for low-temperature superconductors is very narrow, as expressed by the Ginzburg criterion[2]). Additional microscopic terms become irrelevant in this regime.

On the other hand, further away from T_c in the region where the microscopic calculation is valid, additional microscopic contributions may arise (as they do for the conductivity). To reiterate, for the transverse thermoelectric response, we find that they are less divergent than the Aslamazov-Larkin contribution as $T \to T_c$.

To connect the microscopic approach with the critical dynamics, one may expect that in the microscopic approximation, as the temperature is lowered, the Maki-Thompson and density of states terms would become less important as the behavior becomes governed by the stochastic TDGL. For α_{xy}, this clearly occurs in the microscopic calculation.[38] This work thus provides further justification for using the TDGL also as the temperature increases away from T_c into the Gaussian regime (which is the approach taken in Ref. 12).

We note that, in this paper, we assumed that the system is particle-hole symmetric. The conventional result for α_{xy} in a normal metal vanishes under this assumption. We emphasize that this result is not required by particle-hole symmetry. Indeed, in a superconductor, we find that the Aslamazov-Larkin diagrams lead to a finite contribution to α_{xy} above T_c. We have shown that the Maki-Thompson and density of states corrections are less divergent; however, we did not investigate the possibility that these normal-state corrections vanish in the particle-hole symmetric case.

Interest in the Nernst signal has grown recently due to the measurements in high-temperature superconductors, where the fluctuations signal can be observed well above T_c.[10,11] On the other hand, the contribution of superconducting fluctuations to the Nernst signal is yet to be observed in a low-temperature superconductor, for which the BCS microscopics considered in this paper are applicable. As discussed in the Introduction, we expect the fluctuation tail to be observable in the Nernst signal of a suitably chosen superconducting thin film. It would certainly be of interest to verify this prediction experimentally.

ACKNOWLEDGMENTS

I thank Shivaji Sondhi and David Huse, my collaborators on ongoing related work on thermal transport and the Nernst effect in superconductors, for numerous illuminating discussions. I would also like to acknowledge discussions with Vadim Oganesyan and Austen Lamacraft.

[1] W.J. Skocpol and M. Tinkham, Rep. Prog. Phys. **38**, 1049 (1975).
[2] A.I. Larkin and A.A. Varlamov, in *The Physics of Superconductors, Vol 1: Conventional and High-T_c Superconductors*, edited by K.-H. Bennemann and J.B. Ketterson (Springer, Berlin, 2003), p. 95.
[3] D.S. Fisher, M.P.A. Fisher, and D.A. Huse, Phys. Rev. B **43**, 130 (1991).
[4] See, e.g., R.P. Huebener, *Magnetic flux structures in superconductors* (Springer-Verlag, Berlin, 1979), and references therein.
[5] M. Zeh, H.-C. Ri, F. Kober, R.P. Huebener, A.V. Ustinov, J. Mannhart, R. Gross, and A. Gupta, Phys. Rev. Lett. **64**, 3195 (1990); F. Kober, H.-C. Ri, R. Gross, D. Koelle, R.P. Huebener, and A. Gupta, Phys. Rev. B **44**, 11 951 (1991); H.-C. Ri, R. Gross, F. Gollnik, A. Beck, R.P. Huebener, P. Wagner, and H. Adrian, *ibid.* **50**, 3312 (1994).
[6] S.J. Hagen, C.J. Lobb, R.L. Greene, M.G. Forrester, and J. Talvacchio, Phys. Rev. B **42**, 6777 (1990).
[7] J.A. Clayhold, A.W. Linnen, Jr., F. Chen, and C.W. Chu, Phys. Rev. B **50**, 4252 (1994).
[8] C. Hohn, M. Galffy, and A. Freimuth, Phys. Rev. B **50**, 15 875 (1994).
[9] T.T.M. Palstra, B. Batlogg, L.F. Schneemeyer, and J.V. Waszczak, Phys. Rev. Lett. **64**, 3090 (1990).
[10] Z.A. Xu, N.P. Ong, Y. Wang, T. Kakeshita, and S. Uchida, Nature (London) **406**, 486 (2000); Y. Wang, Z.A. Xu, T. Kakeshita, S. Uchida, S. Ono, Y. Ando, and N.P. Ong, Phys. Rev. B **64**, 224519 (2001).
[11] C. Capan, K. Behnia, J. Hinderer, A.G.M. Jansen, W. Lang, C. Marcenat, C. Marin, and J. Flouquet, Phys. Rev. Lett. **88**, 056601 (2002); C. Capan, K. Behnia, Z.Z. Li, H. Raffy, and C. Marin, Phys. Rev. B **67**, 100507 (2003).
[12] I. Ussishkin, S.L. Sondhi, and D.A. Huse, Phys. Rev. Lett. **89**, 287001 (2002).
[13] L.G. Aslamazov and A.I. Larkin, Fiz. Tverd. Tela **10**, 1104 (1968) [Sov. Phys. Solid State **10**, 875 (1968)].
[14] K. Maki, Prog. Theor. Phys. **39**, 897 (1968); **40**, 193 (1968).
[15] R.S. Thompson, Phys. Rev. B **1**, 327 (1970).
[16] Previously this problem was studied using a stochastic TDGL by Ullah and Dorsey.[17] However, as already discussed in Ref. 12, their result for α_{xy} differs from Eq. (3) because their calculation does not account for the contribution of bulk magnetization currents.
[17] S. Ullah and A.T. Dorsey, Phys. Rev. Lett. **65**, 2066 (1990); Phys. Rev. B **44**, 262 (1991).
[18] On the other hand, a *d*-wave symmetry of the order parameter will introduce pair breaking which will suppress the Maki-Thompson contribution to the conductivity. See also S.-K. Yip, Phys. Rev. B **41**, 2612 (1990).
[19] A.A. Varlamov and D.V. Livanov, Zh. Éksp. Teor. Fiz. **99**, 1816 (1991) [Sov. Phys. JETP **72**, 1016 (1991)].
[20] N.R. Cooper, B.I. Halperin, and I.M. Ruzin, Phys. Rev. B **55**, 2344 (1997).
[21] J.M. Luttinger, Phys. Rev. **135**, A1505 (1964).
[22] B.L. Altshuler and A.G. Aronov, in *Electron-Electron Interactions in Disordered Systems*, edited by A.L. Efros and M. Pollak (North-Holland, Amsterdam, 1985), p. 1.
[23] For a diagrammatic treatment of the magnetization, see L.G. Aslamazov and A.I. Larkin, Zh. Éksp. Teor. Fiz. **67**, 647 (1974) [Sov. Phys. JETP **40**, 321 (1974)].
[24] V.N. Popov, *Functional Integrals and Collective Excitations* (Cambridge University Press, Cambridge, 1987).
[25] In the context of superconducting fluctuations, a quantum functional integral approach was used by A.V. Svidzinskii, Teor. Mat. Fiz. **9**, 273 (1971) [Theor. Math. Phys. **9**, 1134 (1971)].
[26] For a recent derivation along these lines, see C.A.R. Sá de Melo, M. Randeria, and J.R. Engelbrecht, Phys. Rev. Lett. **71**, 3202 (1993).
[27] Actually, for our purposes one could also set $Q=0$ from the way the Aslamazov-Larkin diagram is constructed. In the conductivity calculation,[13] the two current vertices have $Q=0$. Here, for α_{xy}, the Aslamazov-Larkin diagram of Fig. 2 (a) has two electric current vertices, one with $Q=0$ and one with a vertex in the $\hat{\mathbf{y}}$ direction, but with $\mathbf{Q}\|\hat{\mathbf{x}}$.
[28] C. Caroli and K. Maki, Phys. Rev. **164**, 591 (1967).
[29] We note that the correct form does have important consequences for the transverse thermoelectric response in a superconductor; I. Ussishkin, S.L. Sondhi, and D.A. Huse (unpublished).
[30] J.S. Langer, Phys. Rev. **128**, 110 (1962).
[31] M.Y. Reizer and A.V. Sergeev, Phys. Rev. B **50**, 9344 (1994). There is a factor of 2 missing in the result for $\mathbf{J}^Q$ in this paper.
[32] B.R. Patton, Phys. Rev. Lett. **27**, 1273 (1971).
[33] J. Keller and V. Korenman, Phys. Rev. Lett. **27**, 1270 (1971); Phys. Rev. B **5**, 4367 (1972).
[34] E. Abrahams, M. Redi, and J.W.F. Woo, Phys. Rev. B **1**, 208 (1970).
[35] D.R. Niven and R.A. Smith, Phys. Rev. B **66**, 214505 (2002).
[36] Here, and in the rest of this section, we use the assumption of particle-hole symmetry in obtaining the powers of electronic blocks containing j_y^Q.
[37] P.C. Hohenberg and B.I. Halperin, Rev. Mod. Phys. **49**, 435 (1977).
[38] A similar observation follows also for the microscopic calculation of the conductivity, albeit in a more subtle manner: The Maki-Thompson term is regularized by pair breaking, and becomes weaker than the Aslamazov-Larkin term as $T\to T_c$. This is true even in the absence of explicit pair breaking.[32,33] In this case, however, not too close to T_c the Maki-Thompson term is an important contribution to the microscopics.